Performance Evaluation of Production Systems Using Real-Time Machine Degradation Signals

Yunyi Kang, *Student Member, IEEE*, Hao Yan, and Feng Ju, *Member, IEEE*

***Abstract*— A machine's degradation status directly influences the operational performance of the production system, such as productivity and product quality. For example, machines associated with different health states may have different remaining life before failure, thus impacting the system throughput. Therefore, it is critical to analyze the coupling between the overall system performance and the machine degradation to better production decision-making, such as maintenance and product dispatch decisions. In this paper, we propose a novel model to evaluate the production performance of a two-machine-and-one-buffer line, given the real-time machine degradation signals. Specifically, a phase-type distribution-based continuous-time Markov chain model is formulated to estimate the system throughput by utilizing the remaining life prediction from the degradation signals. A case study is provided to demonstrate the applicability and effectiveness of the proposed method.**

***Note to Practitioners*—Machine degradation is commonly observed in many industries, such as automotive, semiconductor, and food production, which gradually deteriorates the machine conditions in different operating processes and affects the production system performance. In practice, sensors are largely deployed on the factory floor to monitor the machine's operating condition. However, a gap still exists between machine operating conditions and system performance. In this paper, we develop an analytical model to predict the machine remaining lifetime and estimate the system performance of a small scale production system, using the machine degradation signals from sensors. Furthermore, a Bayesian updating scheme is provided, which enables online evaluation by utilizing the real-time signals. Such a method provides an effective tool for production engineers to analyze the real-time system performance, and further conduct system improvements and control.**

***Index Terms*— Machine degradation, Markov chain, performance evaluation, remaining life.**

I. INTRODUCTION

MANUFACTURING systems, in general, are highly dynamic and coupled with many operations, machines, robots, and material handling devices, which are subject to status degradation. These machines' degradation status directly influences the operational performance of the production system, such as productivity and product quality [1]. For example, machines associated with different health states may have different remaining life before failure, thus impacting system throughput [2]. Therefore, it is critical to analyze the coupling between the overall system performance and the machine degradation to ensure better production decision-making, such as system improvement, maintenance, and product dispatch decisions.

Nevertheless, the changing of machine conditions and random disruption events can influence both instant and long-term system performance [2]. Especially as modern manufacturing systems are becoming more and more complex, system performance evaluation based on real-time system information is more difficult while highly demanded in many industries. For example, in the semiconductor manufacturing systems, accurate prediction of production performance in real time is strongly desired. On the one hand, the mismatch of production capacity and customer orders will lead to heavy back orders, which is costly in such high-yield industries. On the other hand, the production system is typically complex, involving multiple types of equipment and up to several hundred processing operations for each wafer, which themselves may deteriorate at different manners. Therefore, how to evaluate the system performance in real time by incorporating the performance of individual machine units is critically important.

In recent years, thanks to the advances in information and communication technology, sensors are largely deployed on the factory floor which provide unprecedented opportunities to machine degradation information and system operation information in real time, such as machine health status and buffer levels [3]. A degradation signal is defined as a quantity computed from sensor information that captures the current state of the machine and provides information on how that condition is likely to evolve in the future [4]. Machines will fail when the degradation signal reaches a predefined threshold. Typically, the real-time machine degradation processes can be captured through degradation signals from installed sensors. This information nowadays is primarily used for understanding equipment-level or unit-level dynamics to facilitate better maintenance decision-making. Although some research has investigated the influence of machine degradation on the production system performance [2], [5], a significant gap still exists between unit-level analysis and system-level performance evaluation, especially on how to

Manuscript received October 1, 2018; revised January 7, 2019; accepted March 25, 2019. Date of publication June 28, 2019; date of current version January 9, 2020. This work was supported by the National Science Foundation under Grant CMMI-1829238. This paper was recommended for publication by Associate Editor L. Tang and Editor Fan-Tien Cheng upon evaluation of the reviewers' comments. *(Corresponding author: Feng Ju.)*

The authors are with the School of Computing, Informatics, and Decision Systems Engineering, Arizona State University, Tempe, AZ 85281 USA (e-mail: ykang37@asu.edu; haoyan@asu.edu; feng.ju@asu.edu).

Color versions of one or more of the figures in this article are available online at http://ieeexplore.ieee.org.

Digital Object Identifier 10.1109/TASE.2019.2920874

incorporate the real-time degradation signal to better evaluate the system performance.

In this paper, we develop an analytical model to estimate the production performance of a two-machine-and-one-buffer system, given the real-time degradation signals of individual machines. Specifically, a phase-type (PH) distribution-based continuous-time Markov chain model is formulated to estimate the system throughput by utilizing the remaining life prediction from degradation signals. To the best of authors' knowledge, this is the first work on the production system model utilizing the real-time degradation signals for online remaining life prediction and real-time system performance evaluation. Such a model could provide a powerful tool to effectively estimate the system performance in real time by incorporating the degradation process of individual machines and their interactions in the system level.

The rest of this paper is organized as follows: Section II reviews the related literature; Section III describes the problem and provides model assumptions; Section IV derives machine remaining life distributions (RLDs) and converts those to PH distributions using moment matching; Section V develops modeling procedures and Bayesian updating procedures using real-time information; Section VI provides an illustrative case to demonstrate the effectiveness of the method; and Section VII is dedicated to the conclusions and future work. All proofs and detailed derivations are included in the Appendix.

II. Literature Review

For system-level performance evaluation, earlier research works heavily focus on queuing models to estimate the system long-term performance [6]–[8]. In addition, Markovian analysis is also investigated based on the Bernoulli models, geometric models, multi-state models, and exponential models [9]–[11]. However, the strong requirement on machine RLDs in these models is not widely met in the production practice and thus limits the applicability in the industry, according to the empirical and analytical studies [12], [13]. Furthermore, more complex degradation models, such as multi-stage models and multi-factor models, are developed to mimic machine degradation processes in different situations and applications, such as conducting job scheduling and maintenance activities [14]–[18]. Nevertheless, the transition probabilities in these models are assumed to be static, making it difficult to incorporate real-time degradation information. In recent years, the newly developed analytical models focus on flexible transient analysis with system dynamics in real time [19]–[22]. In these models, the adjustable parameters on machine operations and failures are included so that machine degradation conditions can be updated. Zou *et al.* [23] developed a model to continuously update machine conditions and evaluate the system performance by analyzing instant system output using sensors. However, these models do not provide clear guidance on how to update the designated parameters using the real-time degradation signals.

On the other hand, the use of real-time sensing information to predict the degrading machine performance are commonly observed in the reliability and prognostics research. The primary focus is to use degradation signals to understand the equipment's health condition so as to assess its reliability. In the literature, different degradation modeling such as degradation path models [24], random process models [4], and state space models [25] have been developed. There is also research on estimating the degradation signals from a single sensor [4], [26] and multiple sensors [27], [28]. However, such research mainly focuses on individual machines, without further extension to complex manufacturing systems. The closest research related to the problem under investigation in this paper is Hao *et al.* [29], who develops a degradation model for parallel machines to adjust the workloads. However, such model only considers a single stage of the production system and ignores the complication involved with multiple machines and buffers in the real systems.

To the best of authors' knowledge, currently, there is no research combining the real-time machine-level degradation signals and the system-level performance analysis. This paper is intended to bridge the gap between the two research areas as reviewed above.

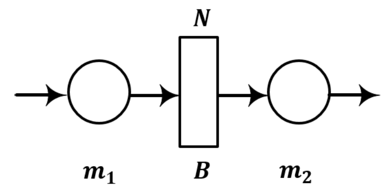

Fig. 1. Two-machine-and-one-buffer system.

III. Problem Description and Assumptions

An illustration of a two-machine-and-one-buffer system is shown in Fig. 1. We use the circles and the rectangle to represent the machines and the buffer, respectively. The arrows in the graph indicate the flow of working parts within the line. The degradation path for each machine is independent of the other machines. Based on the characteristics of machines, buffers and their interactions, the assumptions are addressed as follows.

1) The two machines in the system are denoted as m_1 and m_2. The buffer B has finite capacity N.
2) The two machines operate independently. The processing time (cycle time) for one part at machine k is τ_k, $k = 1, 2$. Similarly, the processing speed (or capacity) for machine m_k is c_k, where $c_k = 1/\tau_k$, $k = 1, 2$. It is assumed that the two machines operate in different processing speeds.
3) Machine m_2 is starved if it is up and the buffer is empty at the beginning of a time slot. Machine m_1 is never starved.
4) Machine m_1 is blocked if it is up and the buffer is full at the beginning of a time slot. Machine m_2 is never blocked.
5) For each machine m_k, the real-time degradation signal $z_k(t)$ is observable or can be estimated in real time to quantify the machine health condition. Furthermore, we also assume a parametric form on the degradation signal $z_k(t) = \eta(\beta_k, \epsilon(t))$. Here, $\eta(\cdot, \cdot)$ is the parameric

model of the degradation signal; β_k is the degradation rate; and $\epsilon(t)$ is the noise of the degradation signal.

6) The failure of machine m_k is assumed to occur when the corresponding degradation signal z_k first passes a predefined failure threshold D_k. At each time, the remaining life R_k is defined as the time from now until machine m_k fails.
7) The repairing time for machine m_k follows an exponential distribution with parameter μ_k, $k = 1, 2$.

To evaluate the production performance, system throughput, the number of parts produced per unit of time, is considered. The problem to be studied in this paper is the following: given the real-time machine degradation signals, develop an approach to continuously evaluate and predict the long-term production performance of two-machine-and-one-buffer systems.

IV. Remaining Life Distribution for Single Machine

A. Derivation of the Remaining Life Distribution

To model the evolution of the general degradation signal, we focus on the degradation signals following the Brownian motion model [29] for each machine k in this paper as shown the following equation:

$$dz_k(t) = \beta_k dt + dW_k(t), \quad k = 1, 2 \tag{1}$$

where $W_k(t)$ is a Brownian motion with variance $\sigma^2 t$.

Given the real-time degradation signal for each machine k, the RLD of machine k can be estimated based on such model. Using (1), the cumulative distribution function (CDF) of the estimated remaining life R_k can be obtained by the inverse Gaussian (IG) distribution [30] as follows:

$$R_k | z_k(t), \beta_k, t \sim \mathrm{IG}(t; \mu_k(t), \lambda_k(t)) \tag{2}$$

where $IG(t; \cdot, \cdot)$ represents the CDF of an IG distribution, with $\mu_k(t) = (D_k - z_k(t))/\beta_k$ and $\lambda_k(t) = (D_k - z_k(t))^2/\sigma_k^2$ are the mean parameter and the shape parameter, respectively. Here, the RLD only depends on the most recent degradation signal $z_k(t)$ and the failure coefficient β_k due to the Markov property of the Brownian motion.

It is worth noting that although the conditional distribution of R_k has been derived, there is no explicit expression of the unconditional RLD, since the integral of β_k does not yield a closed-form solution. For simplicity, we adopt the same techniques in [29], where the maximum *a posteriori* point estimator of β_k at time t, denoted by $\hat{\beta}_k(t)$, is used in estimating the mean parameter as $\mu_k(t) = (D_k - z_k(t))/\hat{\beta}_k(t)$. Besides, the mean and variance of the IG distribution can be computed analytically, as $E(R_k) = \mu_k(t), \mathrm{Var}(R_k) = (\mu_k(t)^3)/(\lambda_k(t))$. Furthermore, the other moments can also be calculated using numerical methods. For other types of degradation signals, the RLD can be similarly derived.

B. Approximation of RLD Using Phase-Type Distributions

Integrating the real-time degradation signal to the system-level modeling is very challenging due to the non-Markovian property of the machine RLD. To address this issue, we propose a new method in this section by estimating the machine RLDs using PH distributions. PH distributions are defined as the time from any of the transient states to the one absorbing state, which connects with the Markovian models [31]. With such transformation, the system performance modeling based on the Markovian model can be thereafter utilized to estimate the system performance. To do this, we will adapt a two-phase PH distribution by introducing two virtual operating states, denoted as state 1 and state 2, and one failure state, denoted as F, for each machine, as shown in Fig. 2.

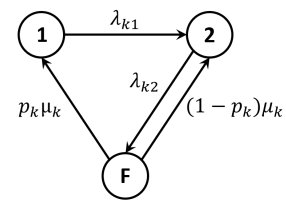

Fig. 2. Modeling machine RLD using PH distributions.

When machine m_k fails, it can be recovered either to state 1 or state 2, with probability $p_k\mu_k$ and $(1 - p_k)\mu_k$ correspondingly. When the machine is in state 1, it can transfer to state 2 with rate λ_{k1}. When the machine is in state 2, it can transfer to state 2 with rate λ_{k2}.

Furthermore, in order to find a PH distribution which has the similar behavior as the IG distribution estimated from the real-time degradation signal, we introduce a moment matching approach. The idea is to match the three moments of the IG distribution and the PH distribution, thus determining the three unknown parameters in the PH distribution. The symbolic expression is shown in the following proposition.

Proposition 1: Given an IG distribution $\mathcal{IG}(\alpha, \beta)$, a corresponding PH distribution, which has the exact format as shown in Fig. 2, can be generated, with parameters as follows.

1) When $(\alpha)/(\beta) > 1$

$$p = \frac{6\alpha\kappa_1 + \sqrt{\kappa_4} - \kappa_2}{\kappa_2 + \sqrt{\kappa_4}}, \lambda_1 = \frac{\kappa_2 + \sqrt{\kappa_4}}{\kappa_3}$$
$$\lambda_2 = \frac{\kappa_2 - \sqrt{\kappa_4}}{\kappa_3} \tag{3}$$

where

$$\kappa_1 = \frac{\alpha^2(\alpha - \beta)}{\beta}, \kappa_2 = \frac{\alpha^3(3\alpha^2 - 2\beta^2)}{\beta^2}$$
$$\kappa_3 = \frac{\alpha^4(3\alpha^2 - \beta^2)}{\beta^2}$$
$$\kappa_4 = \frac{\alpha^6(9\alpha^4 - 18\alpha^3\beta + 6\alpha^2\beta^2 + 6\alpha\beta^3 - 2\beta^4)}{\beta^4}. \tag{4}$$

2) When $(\alpha)/(\beta) = 1$

$$p = 0, \lambda_1 = 0, \lambda_2 = \alpha. \tag{5}$$

3) When $(\alpha)/(\beta) < 1$

$$p = \min(1, \frac{\kappa_5 + \sqrt{\kappa_5^2 + \kappa_5}}{\kappa_6}), \lambda_1 = \lambda_2 = \frac{1 + p}{\alpha} \tag{6}$$

where

$$\kappa_5 = \frac{\alpha^2(\beta - \alpha)}{\beta}, \quad \kappa_6 = \frac{\alpha^2(\beta + \alpha)}{\beta}. \tag{7}$$

Proof: See the Appendix.

Therefore, we can solve the equations generated by the moment matching, thus constructing the PH distribution for a machine's remaining life. It is worth noting that the Proposition 1 can be generalized to other RLDs derived from other types of degradation signals as well.

V. Modeling for Two-Machine-One-Buffer System

A. Two-Machine System Performance Analysis

Using the derived PH distributions for machines' remaining life, a continuous-time and mixed-state Markovian model is developed to estimate the system performance. The state space for the system is defined as the combination of machine states (s_1, s_2), $s_1, s_2 \in \{1, 2, F\}$ and the buffer level h, $h \in [0, N]$, at time t.

To facilitate the derivation, the following notations are introduced.

1) $X_{s_1s_2}(h, t)$: the probability density that machine m_1 in state s_1 and machine m_2 in state s_2, when the buffer occupancy is at h. The buffer level is $h \in (0, N)$, at time t.
2) $Y_{s_1s_2}(N, t)$: the probability density that machine m_1 in state s_1 and machine m_2 in state s_2, when the buffer is full at time t.
3) $Y_{s_1s_2}(0, t)$: the probability density that machine m_1 in state s_1 and machine m_2 in state s_2, when the buffer is zero at time t.

The dynamic transition equations of the probability density functions $X_{s_1s_2}(h, t)$ can be obtained through the integral equations. Taking $X_{11}(\cdot)$ as an example, the probability density function at time $t + \Delta t$ has a summation format with four components as follows.

1) The system stays in the same state from time t to $t+\Delta t$, with probability $X_{11}(h + (c_2 - c_1)\Delta t, t)e^{-(\lambda_{11}+\lambda_{21})\Delta t}$.
2) Machine m_2 remains in the operating state 1 and machine m_1 turns up from down state at time $t+\tau$. The probability can be expressed as: $e^{-\lambda_{21}\Delta t}\int_0^{\Delta t} X_{d1}(h + c_2\Delta t - c_1(\Delta t - \tau), t)p_1\mu_1 e^{-\mu_1\tau}d\tau$.
3) Machine m_1 remains in the operating state 1 and machine m_2 turns up from down state at time $t+\tau$. The probability can be expressed as: $e^{-\lambda_{12}\Delta t}\int_0^{\Delta t} X_{1d}(h + c_2(\Delta t - \tau) - c_1\Delta t, t)p_2\mu_2 e^{-\mu_2\tau}d\tau$.
4) A miscellaneous term representing the deviation of estimation with order $O(\Delta t^2)$.

Furthermore, at most one transition could happen within Δt when it is small enough. Therefore

$$\begin{aligned} &X_{11}(h, t + \Delta t) \\ &= X_{11}(h + (c_2 - c_1)\Delta t, t)e^{-(\lambda_{11}+\lambda_{21})\Delta t} \\ &\quad + e^{-\lambda_{21}\Delta t}\int_0^{\Delta t} X_{d1}(h + c_2\Delta t - c_1(\Delta t - \tau), t)p_1\mu_1 \\ &\quad e^{-\mu_1\tau}d\tau + e^{-\lambda_{12}\Delta t}\int_0^{\Delta t} X_{1d}(h + c_2(\Delta t - \tau) - c_1\Delta t, t) \\ &\quad p_2\mu_2 e^{-\mu_2\tau}d\tau + O(\Delta t^2). \end{aligned} \tag{8}$$

Following the similar idea, we can express all the other $X_{s_1s_2}(h, t)$'s, which are shown in the Appendix.

By simplifying the right-hand side of (8) using Taylor expansion with an accuracy of $O(\Delta t)$, we obtain

$$\begin{aligned} &\frac{X_{11}(h, t + \Delta t) - X_{11}(h, t)}{\Delta t} \\ &= -(\lambda_{11} + \lambda_{21})X_{11}(h, t) \\ &\qquad + (c_2 - c_1)\frac{\partial X_{11}(h, t)}{\partial h} + p_1\mu_1 X_{d1} + p_2\mu_2 X_{1d} + O(\Delta t^2). \end{aligned} \tag{9}$$

When t approaches to zero ($\Delta t \to 0$), an differential equation can be obtained by taking the limit of t as

$$\begin{aligned} &\frac{\partial X_{11}(h, t)}{\partial t} + (c_1 - c_2)\frac{\partial X_{11}(h, t)}{\partial h} \\ &\qquad = -(\lambda_{11} + \lambda_{21})X_{11}(h, t) + p_1\mu_1 X_{d1} + p_2\mu_2 X_{1d}. \end{aligned} \tag{10}$$

Furthermore, since the Markov process is irreducible, we can show that the limiting distributions with regards to t exist. Thus, introducing the following notation:

$$X_{s_1s_2}(h) = \lim_{t\to\infty} X_{s_1s_2}(h, t). \tag{11}$$

Then, (10) can be transformed into the steady-state equation as shown in the following:

$$\begin{aligned} (c_1 - c_2)\frac{\partial X_{11}(h, t)}{\partial h} &= -(\lambda_{11} + \lambda_{21})X_{11}(h, t) \\ &\qquad + p_1\mu_1 X_{d1} + p_2\mu_2 X_{1d}. \end{aligned} \tag{12}$$

Following the similar idea, all the rest steady-state equations can be obtained for all the remaining system states, as illustrated in the Appendix. Then, a matrix form can be generated to express all the steady-state differential equations, as shown in matrix $\mathbf{A_1}$, shown at the bottom of the next page.

In order to find the steady-state distribution $\mathbf{X(h)}$, the following equation has to be solved:

$$\mathbf{c} * \mathbf{X(h)}' = \mathbf{A_1}\mathbf{X(h)} \tag{13}$$

where

$$\begin{aligned} \mathbf{c} = \big[&c_1 - c_2 \quad c_1 - c_2 \quad c_1 \;\; c_1 - c_2 \\ &c_1 - c_2 \quad c_1 \quad -c_2 \quad -c_2 \;\; 0\big]^T \\ \mathbf{X(h)} = \big[&X_{11}(h) \quad X_{12}(h) \quad X_{1d}(h) \;\; X_{21}(h) \quad X_{22}(h) \\ &X_{2d}(h) \quad X_{d1}(h) \quad X_{d2}(h) \quad X_{dd}(h)\big]^T. \end{aligned} \tag{14}$$

The operator ($*$) in (13) represents element-wise multiplication of two vectors. The general solution of the differential equation systems has the following format:

$$\mathbf{X(h)} = \sum_{i=1}^{9} k_i\nu_i e^{\gamma_i h} \tag{15}$$

where γ_i is the eigenvalues, ν_i is the eigenvectors, and k_i is the constants yet to be determined.

The boundary state transition probabilities can be determined by following the similar idea. For boundary probability

$Y_{11}(0, t+\Delta t)$, it can be determined as follows:

$$\begin{aligned} Y_{11}(0, t+\Delta t) = {} & Y_{11}(0,t)e^{-(\lambda_{11}+\lambda_{21})\Delta t} \\ & + \int_0^{(c_2-c_1)\Delta t} X_{11}(h,t)e^{-(\lambda_{11}+\lambda_{21})\Delta t}dh \\ & + \int_0^{\Delta t} Y_{d1}(0,t)p_1\mu_1 e^{-\mu_1\tau}d\tau + O(\Delta t^2). \end{aligned} \tag{16}$$

Similar equations for other states are shown in the Appendix. Therefore, we can simplify these equations and put them into matrix $\mathbf{A_2}$, shown at the bottom of this page. The values of all entries in $\mathbf{Y(0)}$ can be obtained by solving the matrix equation

$$\mathbf{A_2Y(0)} = \mathbf{c_2} * \mathbf{X(0)} \tag{17}$$

where

$$\begin{aligned} \mathbf{c_2} &= \begin{bmatrix} c_1-c_2 & c_1-c_2 & c_1-c_2 \\ c_1-c_2 & -c_2 & -c_2 & 0 \end{bmatrix}^T \\ \mathbf{Y(0)} &= \begin{bmatrix} Y_{11}(0) & Y_{12}(0) & Y_{21}(0) & Y_{22}(0) \\ Y_{d1}(0) & Y_{d2}(0) & Y_{dd}(0) \end{bmatrix}^T \\ \mathbf{X(0)} &= \begin{bmatrix} X_{11}(0) & X_{12}(0) & X_{21}(0) & X_{22}(0) \\ X_{d1}(0) & X_{d2}(0) & X_{dd}(0) \end{bmatrix}^T. \end{aligned} \tag{18}$$

Similarly, we can get the boundary condition when the buffer is full

$$\begin{aligned} Y_{11}(N, t+\Delta t) = {} & Y_{11}(N,t)e^{-(\lambda_{11}+\lambda_{21})\Delta t} \\ & + \int_0^{(c_1-c_2)\Delta t} X_{11}(N-h,t)e^{-(\lambda_{11}+\lambda_{21})\Delta t}dh \\ & + \int_0^{\Delta t} Y_{1d}(N,t)p_2\mu_2 e^{-\mu_2\tau}d\tau + O(\Delta t^2). \end{aligned} \tag{19}$$

Simplifications for other states when the buffer is full are also shown in the Appendix. Similarly, we can use matrix $\mathbf{A_3}$, shown at the bottom of this page, to represent the parameters in the equations containing $\mathbf{Y(N)}$.

Therefore, the values of all entries in $\mathbf{Y(N)}$ can be obtained by solving the following matrix equation:

$$\mathbf{A_3Y(N)} = -\mathbf{c_3} * \mathbf{X(N)} \tag{20}$$

where

$$\begin{aligned} \mathbf{c_3} &= \begin{bmatrix} c_1-c_2 & c_1-c_2 & c_1 \\ c_1-c_2 & c_1-c_2 & c_1 & 0 \end{bmatrix}^T \\ \mathbf{Y(N)} &= \begin{bmatrix} Y_{11}(N) & Y_{12}(N) & Y_{1d}(N) & Y_{21}(N) \\ Y_{22}(N) & Y_{d2}(N) & Y_{dd}(N) \end{bmatrix}^T \\ \mathbf{X(N)} &= \begin{bmatrix} X_{11}(N) & X_{12}(N) & X_{1d}(N) & X_{21}(N) \\ X_{22}(N) & X_{d2}(N) & X_{dd}(N) \end{bmatrix}^T. \end{aligned} \tag{21}$$

Notice that the values in $\mathbf{X(0)}$ and $\mathbf{X(N)}$ are the special solutions in (15) when $h = 0$ and $h = N$, respectively.

In order to find the values of all k's in (15), the particular solution of (17) and (20) will be found. First, notice that the summation of all the probabilities should be equal to one:

$$\int_0^N X_{.}(h)dh + Y_{.}(0) + Y_{.}(N) = 1. \tag{22}$$

Furthermore, in the long run, when the first machine is faster, and both machines are operating, the buffer level cannot always be zero. On the other hand, if the second machine is faster, the buffer level cannot always be full. Therefore, we have the following conditions:

1) If $c_1 > c_2$

$$Y_{11}(0)=0,\ \ Y_{12}(0)=0,\ \ Y_{21}(0)=0,\ \ Y_{22}(0)=0. \tag{23}$$

$$\mathbf{A}_1 = \begin{bmatrix} -(\lambda_{11}+\lambda_{21}) & 0 & p_2\mu_2 & 0 & 0 & 0 & p_1\mu_1 & 0 & 0 \\ \lambda_{21} & -(\lambda_{11}+\lambda_{22}) & (1-p_2)\,\mu_2 & 0 & 0 & 0 & 0 & p_1\mu_1 & 0 \\ 0 & \lambda_{22} & -(\lambda_{11}+\mu_2) & 0 & 0 & 0 & 0 & 0 & p_1\mu_1 \\ \lambda_{11} & 0 & 0 & -(\lambda_{12}+\lambda_{21}) & 0 & p_2\mu_2 & (1-p_1)\,\mu_1 & 0 & 0 \\ 0 & \lambda_{11} & 0 & \lambda_{21} & -(\lambda_{12}+\lambda_{22}) & (1-p_2)\,\mu_2 & 0 & (1-p_1)\,\mu_1 & 0 \\ 0 & 0 & \lambda_{11} & 0 & \lambda_{22} & -(\lambda_{12}+\mu_2) & 0 & 0 & (1-p_1)\,\mu_1 \\ 0 & 0 & 0 & \lambda_{12} & 0 & 0 & -(\mu_1+\lambda_{21}) & 0 & p_2\mu_2 \\ 0 & 0 & 0 & 0 & \lambda_{12} & 0 & \lambda_{21} & -(\mu_1+\lambda_{22}) & (1-p_2)\,\mu_2 \\ 0 & 0 & 0 & 0 & 0 & \lambda_{12} & 0 & \lambda_{22} & -(\mu_1+\mu_2) \end{bmatrix}$$

$$\mathbf{A}_2 = \begin{bmatrix} -(\lambda_{11}+\lambda_{21}) & 0 & 0 & 0 & p_1\mu_1 & 0 & 0 \\ \lambda_{21} & -(\lambda_{11}+\lambda_{22}) & 0 & 0 & 0 & p_1\mu_1 & 0 \\ \lambda_{11} & 0 & -(\lambda_{12}+\lambda_{21}) & 0 & (1-p_1)\,\mu_1 & 0 & 0 \\ \lambda_{11} & 0 & -(\lambda_{12}+\lambda_{21}) & 0 & (1-p_1)\,\mu_1 & 0 & 0 \\ 0 & \lambda_{11} & \lambda_{21} & -(\lambda_{12}+\lambda_{22}) & 0 & (1-p_1)\,\mu_1 & 0 \\ 0 & 0 & \lambda_{12} & 0 & -(\mu_1+\lambda_{21}) & 0 & p_2\mu_2 \\ 0 & 0 & 0 & \lambda_{12} & \lambda_{21} & -(\mu_1+\lambda_{22}) & (1-p_2)\,\mu_2 \\ 0 & 0 & 0 & 0 & 0 & \lambda_{22} & -(\mu_1+\mu_2) \end{bmatrix}$$

$$\mathbf{A}_3 = \begin{bmatrix} -(\lambda_{11}+\lambda_{21}) & 0 & p_2\mu_2 & 0 & 0 & 0 & 0 \\ \lambda_{21} & -(\lambda_{11}+\lambda_{22}) & (1-p_2)\,\mu_2 & 0 & 0 & 0 & 0 \\ 0 & \lambda_{22} & -(\lambda_{11}+\mu_2) & 0 & 0 & 0 & p_1\mu_1 \\ \lambda_{11} & 0 & 0 & -(\lambda_{12}+\lambda_{21}) & 0 & p_2\mu_2 & 0 \\ 0 & \lambda_{11} & 0 & \lambda_{21} & -(\lambda_{12}+\lambda_{22}) & (1-p_2)\,\mu_2 & 0 \\ 0 & 0 & \lambda_{11} & 0 & \lambda_{22} & -(\lambda_{12}+\mu_2) & (1-p_1)\,\mu_1 \\ 0 & 0 & 0 & 0 & 0 & \lambda_{12} & -(\mu_1+\mu_2) \end{bmatrix}$$

TABLE I
NUMERICAL RESULTS

Case	m_1					m_2					N	$\widehat{PR}$	PR_{sim}	Δ
	β_1	σ_1	z_1	r_1	c_1	β_2	σ_2	z_2	r_2	c_2				
1	0.47	0.64	4.58	1.08	1.50	0.61	0.24	6.11	1.42	0.98	5	0.4831	0.4881	-1.02%
2	0.42	0.20	4.90	1.33	1.96	0.63	0.84	4.04	1.35	0.88	2	0.5857	0.5850	-0.11%
3	0.29	0.30	6.29	0.76	1.19	1.12	0.60	2.63	1.12	1.86	3	0.9581	0.9520	0.64%
4	0.97	0.60	4.31	1.18	1.60	0.39	0.57	5.01	1.44	0.83	8	0.7556	0.7556	0.00%
5	0.21	0.02	6.54	0.95	1.36	0.28	0.04	6.54	0.66	1.75	3	0.9600	0.9358	-2.52%
6	0.92	0.44	4.12	0.64	1.46	0.77	0.59	3.72	0.32	1.16	8	0.7003	0.6831	2.52%
7	0.73	0.20	3.59	0.36	1.83	0.65	0.39	3.69	0.30	1.53	4	0.8455	0.8346	1.30%
8	0.61	0.78	5.34	1.37	1.39	0.37	0.30	5.98	1.41	0.93	7	0.5950	0.5892	-0.98%
9	0.79	0.39	3.33	1.38	1.63	0.72	0.10	5.04	0.45	1.45	6	0.9378	0.9296	0.88%
10	0.47	0.17	5.88	1.45	0.85	0.58	0.78	5.15	1.28	1.58	6	0.6201	0.6052	-2.40%
11	0.64	0.43	5.04	1.34	1.44	0.44	0.07	6.67	0.27	1.16	7	0.5155	0.5168	-0.26%
12	0.20	0.07	6.71	1.24	1.50	0.42	0.53	6.01	0.85	1.22	3	0.9711	0.9630	0.84%
13	0.60	0.20	5.07	0.80	1.72	0.64	0.98	3.18	0.62	1.64	8	1.2128	1.1935	1.62%
14	0.59	0.27	4.53	0.75	1.48	0.58	0.34	4.43	0.39	1.69	2	1.0055	0.9897	1.59%
15	0.25	0.06	6.31	1.34	1.45	0.62	0.32	4.29	1.31	1.02	3	0.8973	0.8968	0.05%
16	0.30	0.27	6.11	1.37	1.94	0.53	0.03	5.86	0.64	1.67	5	0.9329	0.9225	-1.11%
17	0.21	0.06	7.03	0.25	1.66	0.44	0.12	5.89	0.68	1.42	6	0.7305	0.7173	1.83%
18	0.58	0.05	4.28	0.22	1.56	0.76	0.89	4.05	1.13	1.37	6	0.8328	0.8130	2.44%
19	0.33	0.39	6.93	0.53	1.13	0.51	0.10	5.47	0.30	1.14	8	0.6539	0.6689	-2.25%
20	0.52	0.40	5.00	0.54	1.46	0.54	0.49	4.39	0.76	1.61	7	1.0442	1.0358	0.81%

2) If $c_1 < c_2$

$$Y_{11}(N)=0,\quad Y_{12}(N)=0,\quad Y_{21}(N)=0,\quad Y_{22}(N)=0. \tag{24}$$

Following the procedures mentioned above, the steady-state distribution for all the states can be determined, and thus, the system throughput can be determined as follows:

$$TP = c_2 \sum_{s_1\in\{1,2\}} \sum_{s_2\in\{1,2\}} \left(\int_0^N (X_{s_1 s_2}(h) + X_{ds_2}(h))dh + c_1 Y_{s_1 s_2}(0) + c_2 Y_{s_1 s_2}(N) \right). \tag{25}$$

The system throughput is calculated by adding up the throughput in all states, which is expressed as the throughput of a given system state times the probability that the system in the state. In (25), the throughput is expressed with three situations: when the buffer is between 0 and N, when the buffer is empty and machine 2 is faster, and when the buffer is full and machine 1 is faster.

B. Bayesian Updating

After the RLD and the system throughput is estimated, we need to perform the real-time update on the machine remaining life $R_k, k = 1, 2$ and the system throughput TP with real-time data.

Before updating the online Bayesian, we need to conduct the offline analysis. To do so, we need to collect the degradation signals over the different cycles $i = 1, \cdots, n$ for each machine k. We can then estimate the mean and covariance of the degradation coefficient β_k based on the n time points as sample mean $\kappa_{k,0} = (1/(n) \sum_{i=1}^{n} \beta_{k,i}$ and sample variance $\tau_{k,0}^2 = (1)/(n) \sum_{i=1}^{n} (\beta_{k,i} - \kappa_{k,0})^2$. When collecting the real-time sensing data for machine condition $z_k(t)$, we first know that the increment of the degradation signal follows the Gaussian distribution as $\delta z_k(t)|\beta_k \sim N(\beta_k \delta t, \sigma_k^2 \delta t)$ by the property of Brownian motion. By the Markov property, we know all the nonoverlapping incremental of the degradation signals $\delta z_k(1), \cdots, \delta z_k(t)$ are statistical independent. Therefore, the likelihood can be derived as $p(\delta z_k(1), \cdots, \delta z_k(t)|\beta_k) = \prod_{i=1}^{t} p(\delta z_k(i)|\beta_k)$. Finally, the posterior distribution can be derived as $\beta_k|\delta z_k(t) \sim N(\kappa_k(t), \tau_k^2(t))$, with the posterior mean $\kappa_k(t) = (\tau_k^2 \sum_{i=1}^{t} \delta z_k(i) + \kappa_{k,0}\sigma_k^2)/(\tau_k^2 t + \sigma_k^2)$ and posterior variance $\tau_k^2(t) = (\sigma_k^2 \tau_{k,0})/(\tau_{k,0}^2 t + \sigma_k^2)$, where the $\kappa_{k,0}$ and $\tau_{k,0}^2$ are the prior mean and variance, respectively.

C. Validation

In order to evaluate the system performance of the model, simulation experiments have been conducted. The system parameters are randomly generated using the following procedure.

Procedure 1:

1) Set up machine capacity $c_k \in (0.5, 2), k = 1, 2$ and buffer level $N \in \{2, \ldots, 8\}$.
2) Set up machine repair rate $r_k \in (0.2, 1.8), k = 1, 2$.
3) Set up the predefined degradation threshold $D_k = 8$, $k = 1, 2$.
4) Set up machine degradation level $z_k \in (0, 5), k = 1, 2$.
5) Set up degradation rate $\beta_k \in (0, 1)$ and noise standard deviation $\sigma_k \in (0, 1)$, $k = 1, 2$.

All the simulation cases are conducted with 50 replications and 20 000 simulation length. The performance measurement adopted is the relative production performance difference between the analytical model and the simulation experiments

$$\Delta = \frac{\widehat{\mathrm{PR}} - \mathrm{PR}_{\mathrm{sim}}}{\mathrm{PR}_{\mathrm{sim}}} \times 100\%$$

where $\mathrm{PR}_{\mathrm{sim}}$ is the simulation results, and $\widehat{\mathrm{PR}}$ is the analytical solution to the model. Numerical examples are shown in Table I.

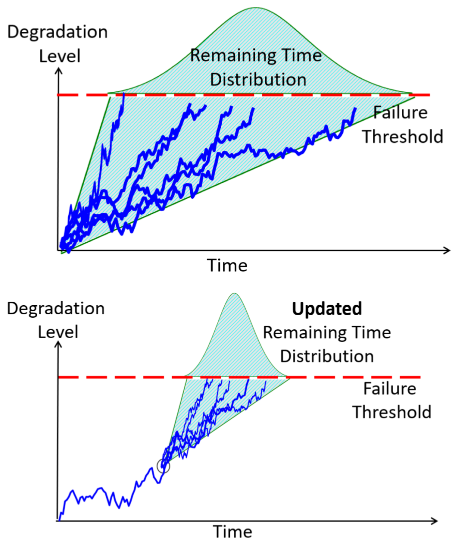

Fig. 3. Degradation signals and predicted remaining life prediction.

Furthermore, we conduct 500 simulation experiments to test the performance of the analytical comparing to the simulation results. For most of the cases, the Δ-measure is below 1%. For the cases with production rate under 0.7, the average relative difference is below 5%. There are extremely rare cases (under 1% of the total experiments) that the Δ-measure is over 10%. They occur when the degradation level of a machine is very close to the predefined threshold. Under these scenarios, the throughput is very low, i.e., less than 0.2. However, for these cases, the absolute difference between the simulation and the analytical results is within 0.03. These results can show that our method can effectively evaluate the system performance.

VI. Case Study

To demonstrate the effectiveness of the method, a case study is provided to evaluate a two-machine-one-buffer system's performance with real machine degradation signals. To ensure the confidentiality of the data, all the data and parameters introduced below have been modified and are used for illustration purpose only.

The data set we use for the real-time degradation signals includes 21 bearing samples. These degradation signals are calculated from the original vibration signals, captured by an accelerometer, to track the evolution of the vibration level with respect to time [4]. A failure threshold of the degradation signals is set according to the industrial standard [32]. Even though the experiments are conducted on a set of identical thrust ball bearings in an accelerated testing, the time-to-failure for all samples are quite different, ranging from 100 to 300 cycles, with a sampling interval of 2 min per cycle. The differences are mainly due to the sample-to-sample variation and the environmental uncertainty.

The remaining life prediction can be estimated and updated online using the real-time degradation signal. Fig. 3 shows the illustration of the predicted RLD. From Fig. 3, we can observe that, initially, the RLD has a large variance. After observing more degradation signals, the updated remaining life presents a much smaller variance, which shows the power of observing more real-time degradation signals.

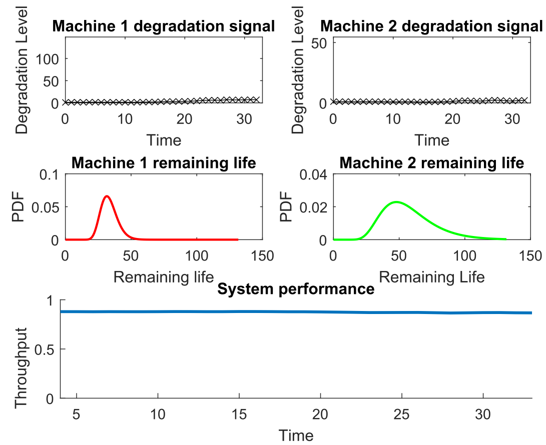

Fig. 4. System performance evaluation when two machines are in the good operating state. The degradation signal plots record the degradation level read from the signals. Machine remaining life plots depict the probability density function of the distribution, given the current degradation level estimated using (2). The system performance chart plots the throughput obtained using the method in Section V.

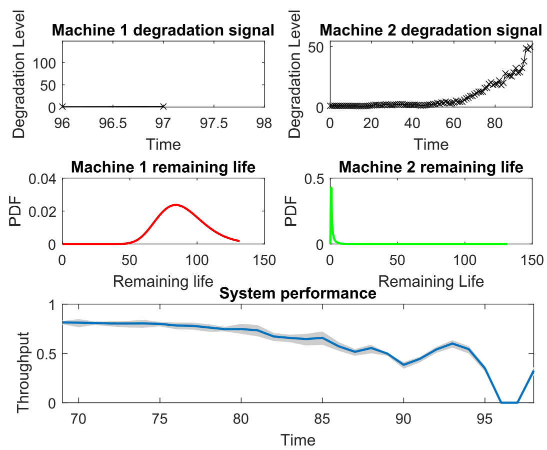

Fig. 5. System performance evaluation when machine m_2 in inferior operating state. The degradation signal plots record the degradation level read from the signals. Machine remaining life plots depict the probability density function of the distribution given the current degradation level estimated using (2). The system performance chart plots the throughput line obtained using the method in Section V, with the 95% confidence interval simulation plots displayed as the shaded area.

Finally, we will discuss the system throughput at different stages of machine health status. Fig. 4 shows the system status at initial stages (e.g., the system operates less than 50 cycles), where both machines are in good operating states, with low degradation level. The average of the remaining time for both machines are large, according to the RLD. Therefore, the system throughput is high. Theoretically, over the long run, the throughput cannot be larger than the minimum capacity in the system, which is known as the bottleneck. In this case, the minimum capacity is 0.9 for machine m_2. Since the machine is less likely to fail in short time, the estimated system throughput is very close to the theoretical upper bound 0.9. When machine 2 approaches to the threshold (e.g., shown in Fig. 5 at $t = 95$), the estimated system performance drops significantly. Since the single machine degradation process is not monotone, it can be observed that throughput ramps up when the status of a machine recovers in a short period of time. For example, between time 90 and 100 as shown in Fig. 5, there is a decrease on the degradation level of machine 1. The system throughput, similarly, shows an increase between time 90 and 95 due to the recovery of machine status. However, when either the machine fails, over the long run, the estimated production rate is zero, even though for short time, there might be output due to the remaining parts in the buffer. The throughput will be zero when the failed machine is under repair and then ramps up when both machines are under operations.

VII. Conclusion

In this paper, we develop a novel analytical model to evaluate the system performance of a two-machine-and-one-buffer line given real-time machine degradation signals. Specifically, PH distributions are generated to mimic the RLD of each machine, and a continuous time Markovian model is formulated to estimate the system throughput. A case study is included to demonstrate the effectiveness of the proposed method.

In practice, the method can be applied for the system performance monitor, diagnostics, prognostics, and control for a variety of production systems. Practitioners can obtain the real-time evaluations and predictions of the system production performance. This method can provide not only a better understanding of individual machines, such as degradation level and the remaining useful life, but also their impact on the overall production system performance. The results can contribute to the other operational activities, such as production scheduling and maintenance.

Future work can be dedicated to extending such a model to more complicated production systems, such as longer lines or assembly systems. The complicated system dynamics of these systems will expose great challenges to the system modeling and computational efficiency so that sophisticated approximation methods should be pursued. Then, the developed approach can be easily generalized to other types of degradation signals, modeled by stochastic processes other than Brownian motion, to enhance the model's efficacy in a variety of practical systems. These data from multiple sensors can be incorporated into the model, which can provide additional information and therefore possibly improve the quality of the machine condition assessment. In addition, future research efforts could be dedicated to investigating system improvement and control policies based on real-time data on the factory floor.

Appendix

A. *Proof of Proposition* 1

Let Y denote a random variable, presenting the time staying in the system. Then, the moment generating function of this variable, noted as $M_Y(t)$, can be expressed as follows:

$$\begin{aligned} M_Y(t) &= \mathbf{E}(e^{tY}) = \int_{-\infty}^{\infty} e^{ty} f(y)dy \\ &= p\int_0^{\infty} e^{ty_1}e^{-\lambda_1 y_1}dy_1 \int_0^{\infty} \lambda_2 e^{-\lambda_2 y_2}dy_2 \\ &\quad + (1-p)\int_0^{\infty} e^{ty_2}\lambda_2 e^{-\lambda_2 y_2}dy_2 \\ &= p\frac{\lambda_1}{\lambda_1 - t}\frac{\lambda_2}{\lambda_2 - t} + (1-p)\frac{\lambda_2}{\lambda_2 - t}. \end{aligned} \tag{26}$$

Therefore, we can get the three moments of Y as follows:

$$\begin{aligned} m_1 &= \frac{dM_Y(t)}{dt}|_{t=0} = \frac{p}{\lambda_1} + \frac{1}{\lambda_2} \\ m_2 &= \frac{d^2M_Y(t)}{dt^2}|_{t=0} = \frac{2p}{\lambda_1^2} + \frac{2p}{\lambda_1\lambda_2} + \frac{2}{\lambda_2^2} \\ m_3 &= \frac{d^3M_Y(t)}{dt^3}|_{t=0} = \frac{6p}{\lambda_1^3} + \frac{6p}{\lambda_1^2\lambda_2} + \frac{6p}{\lambda_1\lambda_2^2} + \frac{6}{\lambda_2^3}. \end{aligned} \tag{27}$$

Let ϕ_1,ϕ_2, and ϕ_3 be the first three moment of the IG distribution $\mathcal{IG}(\alpha, \beta)$. By using the moment generating function of IG distributions, we can find the value of the ϕ's as follows:

$$\begin{aligned} \phi_1 &= \alpha \\ \phi_2 &= \frac{\alpha^2(\alpha + \beta)}{\beta} \\ \phi_3 &= \frac{\alpha^3(\beta^2 + 3\beta\alpha + 3\alpha^2)}{\beta^2}. \end{aligned} \tag{28}$$

Therefore, we can solve the equations generated by matching the moments of the IG distribution and the PH distribution, thus determining the three unknown parameters in the PH distribution.

It can be verified that real solutions exist if and only if when $\alpha \geq \beta$. Specifically, when $\alpha = \beta$ and $p = 0$, the phase-type distribution obtained is an exponential distribution.

When $\alpha < \beta$, matching three moments is not possible because no feasible solution exists. Rather, we match two moments for the distribution. In this case, three variables are in the PH distribution while only two moment functions are available for the moment matching. In other words, it is possible to have multiple feasible parameter settings to match an IG distribution into the PH distribution. In this paper, we provide only one special solution to find the parameters in the PH distribution

$$\begin{aligned} \kappa_5 &= 2m_1^2 - m_2 \\ p &= \min(1, \frac{\kappa_5 + \sqrt{\kappa_5^2 + \kappa_5}}{m_2}) \\ \lambda_1 &= \lambda_2 = \frac{1+p}{m_1}. \end{aligned} \tag{29}$$

It can be verified that the λ and p values are feasible for all the situations when $\alpha < \beta$.

B. *Dynamic and Steady-State Equations*

Following the similar idea as in (8), we can derive the dynamic equations for all the other $X_{s_1 s_2}(h, t)$

as follows:

$$
\begin{aligned}
&X_{12}(h, t+\Delta t) \\
&= X_{12}(h+(c_2-c_1)\Delta t, t)e^{-(\lambda_{11}+\lambda_{22})\Delta t} \\
&\quad + e^{-\lambda_{22}\Delta t}\int_0^{\Delta t} X_{d2}(h+c_2\Delta t - c_1(\Delta t-\tau), t)p_1\mu_1 \\
&\quad \times e^{-\mu_1\tau}d\tau + e^{-\lambda_{11}\Delta t}\int_0^{\Delta t} X_{1d}(h+c_2(\Delta t-\tau) \\
&\quad - c_1\Delta t, t)(1-p_2)\mu_2 e^{-\mu_2\tau}d\tau + e^{-\lambda_{11}\Delta t}\int_0^{\Delta t} X_{11}(h \\
&\quad + (c_2-c_1)\Delta t, t)\lambda_{11}e^{-\lambda_{11}\tau}d\tau + O(\Delta t^2) \qquad (30)
\end{aligned}
$$

$$
\begin{aligned}
&X_{1d}(h, t+\Delta t) \\
&= X_{1d}(h-c_1\Delta t, t)e^{-(\lambda_{11}+\mu_2)\Delta t} \\
&\quad + e^{-\mu_2\Delta t}\int_0^{\Delta t} X_{dd}(h-c_1(\Delta t-\tau), t)p_1\mu_1 e^{-\mu_1\tau}d\tau \\
&\quad + e^{-\lambda_{11}\Delta t}\int_0^{\Delta t} X_{12}(h+c_2(\Delta t-\tau)-c_1\Delta t, t)\lambda_{22} \\
&\quad e^{-\lambda_{22}\tau}d\tau + O(\Delta t^2) \qquad (31)
\end{aligned}
$$

$$
\begin{aligned}
&X_{21}(h, t+\Delta t) \\
&= X_{21}(h+(c_2-c_1)\Delta t, t)e^{-(\lambda_{12}+\lambda_{21})\Delta t} \\
&\quad + e^{-\lambda_{11}\Delta t}\int_0^{\Delta t} X_{d1}(h+c_2\Delta t-c_1(\Delta t-\tau), t)(1-p_1) \\
&\quad \times \mu_1 e^{-\mu_1\tau}d\tau + e^{-\lambda_{11}\Delta t}\int_0^{\Delta t} X_{11}(h+(c_2-c_1)\Delta t, t) \\
&\quad \times \lambda_{11}e^{-\lambda_{11}\tau}d\tau + e^{-\lambda_{12}\Delta t}\int_0^{\Delta t} X_{2d}(h-c_1\Delta t \\
&\quad + c_2(\Delta t-\tau), t)p_2\mu_2 e^{-\mu_2\tau}d\tau + O(\Delta t^2) \qquad (32)
\end{aligned}
$$

$$
\begin{aligned}
&X_{22}(h, t+\Delta t) \\
&= X_{22}(h+(c_2-c_1)\Delta t, t) \\
&\quad \times e^{-(\lambda_{12}+\lambda_{21})\Delta t} + e^{-\lambda_{22}\Delta t}\int_0^{\Delta t} X_{12}(h+(c_2-c_1)\Delta t, t) \\
&\quad \times p_1\lambda_{11}e^{-\lambda_{11}\tau}d\tau + e^{-\lambda_{22}\Delta t}\int_0^{\Delta t} X_{d2}(h+c_2\Delta t-c_1 \\
&\quad \times (\Delta t-\tau), t)(1-p_1)\mu_1 e^{-\mu_1\tau}d\tau + e^{-\lambda_{12}\Delta t}\int_0^{\Delta t} X_{21} \\
&\quad \times (h+(c_2-c_1)\Delta t, t)p_1\lambda_{21}e^{-\lambda_{21}\tau}d\tau + e^{-\lambda_{12}\Delta t} \\
&\quad \times \int_0^{\Delta t} X_{2d}(h+c_2(\Delta t-\tau)-c_1\Delta t, t)(1-p_2)\mu_2 e^{-\mu_2\tau}d\tau. \qquad (33)
\end{aligned}
$$

The simplified steady-state dynamic equation, following the idea of (11) and (12), is shown as follows:

$$
\begin{aligned}
(c_1-c_2)\frac{\partial X_{12}(h)}{\partial h} &= -(\lambda_{11}+\lambda_{22})X_{12}(h) \\
&\quad + p_1\mu_1 X_{d2}(h) + (1-p_2)\mu_2 X_{1d}(h) \qquad (34)
\end{aligned}
$$

$$
\begin{aligned}
c_1\frac{\partial X_{1d}(h)}{\partial h} &= -(\lambda_{11}+\mu_2)X_{1d}(h) \\
&\quad + p_1\mu_1 X_{dd}(h) + \lambda_{12}X_{12}(h) \qquad (35)
\end{aligned}
$$

$$
\begin{aligned}
(c_1-c_2)\frac{\partial X_{21}(h)}{\partial h} &= -(\lambda_{12}+\lambda_{21})X_{12}(h) \\
&\quad + \lambda_{11}X_{11}(h) + p_2\mu_2 X_{2d}(h) \\
&\quad + (1-p_1)\mu_1 X_{d1}(h) \qquad (36)
\end{aligned}
$$

$$
\begin{aligned}
(c_1-c_2)\frac{\partial X_{22}(h)}{\partial h} &= -(\lambda_{12}+\lambda_{22})X_{12}(h) \\
&\quad + \lambda_{11}X_{12}(h) + \lambda_{21}X_{21}(h) + (1-p_2) \\
&\quad \times \mu_2 X_{2d}(h) + (1-p_1)\mu_1 X_{d2}(h) \qquad (37)
\end{aligned}
$$

$$
\begin{aligned}
c_1\frac{\partial X_{2d}(h)}{\partial h} &= -(\lambda_{12}+\mu_2)X_{12}(h) \\
&\quad + \lambda_{11}X_{d2}(h) + \lambda_{22}X_{22}(h) \\
&\quad + (1-p_1)\mu_1 X_{dd}(h) \qquad (38)
\end{aligned}
$$

$$
\begin{aligned}
-c_2\frac{\partial X_{d1}(h)}{\partial h} &= -(\mu_1+\lambda_{21})X_{d1}(h) \\
&\quad + \lambda_{12}X_{21}(h) + p_2\mu_2 X_{dd}(h) \qquad (39)
\end{aligned}
$$

$$
\begin{aligned}
-c_2\frac{\partial X_{d2}(h)}{\partial h} &= -(\mu_1+\lambda_{22})X_{d2}(h) \\
&\quad + \lambda_{12}X_{22}(h) + \lambda_{21}X_{d1}(h) \\
&\quad + (1-p_2)\mu_2 X_{dd}(h) \qquad (40)
\end{aligned}
$$

$$
\begin{aligned}
0 &= -(\mu_1+\mu_2)X_{dd}(h) \\
&\quad + \lambda_{12}X_{2d}(h) + \lambda_{22}X_{d2}(h). \qquad (41)
\end{aligned}
$$

The following equations determine the boundary conditions:

$$
\begin{aligned}
&Y_{12}(0, t+\Delta t) \\
&\quad = Y_{12}(0, t)e^{-(\lambda_{11}+\lambda_{22})\Delta t} \\
&\qquad + \int_0^{(c_2-c_1)\Delta t} X_{12}(h, t)e^{-(\lambda_{11}+\lambda_{22})\Delta t}dh \\
&\qquad + \int_0^{\Delta t} Y_{d2}(0, t)p_1\mu_1 e^{-\mu_1\tau}d\tau + \int_0^{\Delta t} Y_{11}(0, t)\lambda_{21} \\
&\qquad \times e^{-\lambda_{21}\tau}d\tau + O(\Delta t^2) \qquad (42)
\end{aligned}
$$

$$
Y_{1d}(0, t) = 0 \qquad (43)
$$

$$
\begin{aligned}
&Y_{21}(0, t+\Delta t) \\
&\quad = Y_{21}(0, t)e^{-(\lambda_{12}+\lambda_{21})\Delta t} \\
&\qquad + \int_0^{(c_2-c_1)\Delta t} X_{21}(h, t)e^{-(\lambda_{12}+\lambda_{21})\Delta t}dh \\
&\qquad + \int_0^{\Delta t} Y_{11}(0, t)\lambda_{11}e^{-\lambda_{11}\tau}d\tau + \int_0^{\Delta t} Y_{d1}(0, t) \\
&\qquad \times (1-p_1)\mu_1 e^{-\mu_1\tau}d\tau + O(\Delta t^2) \qquad (44)
\end{aligned}
$$

$$
\begin{aligned}
&Y_{22}(0, t+\Delta t) \\
&\quad = Y_{22}(0, t)e^{-(\lambda_{12}+\lambda_{22})\Delta t} \\
&\qquad + \int_0^{(c_2-c_1)\Delta t} X_{22}(h, t)e^{-(\lambda_{12}+\lambda_{22})\Delta t}dh \\
&\qquad + \int_0^{\Delta t} Y_{12}(0, t)\lambda_{11}e^{-\lambda_{11}\tau}d\tau + \int_0^{\Delta t} Y_{d2}(0, t) \\
&\qquad (1-p_1)\mu_1 e^{-\mu_1\tau}d\tau \\
&\qquad + \int_0^{\Delta t} Y_{21}(0, t)\lambda_{21}e^{-\lambda_{21}\tau}d\tau + O(\Delta t^2) \qquad (45)
\end{aligned}
$$

$$
Y_{2d}(0, t) = 0 \qquad (46)
$$

$$
\begin{aligned}
&Y_{d1}(0, t+\Delta t) \\
&\quad = Y_{d1}(0, t)e^{-(\mu_1+\lambda_{21})\Delta t} \\
&\qquad + \int_0^{c_2\Delta t} X_{d1}(h, t)e^{-(\mu_1+\lambda_{21})\Delta t}dh \\
&\qquad + \int_0^{\Delta t} Y_{21}(0, t)\lambda_{12}e^{-\lambda_{12}\tau}d\tau + \int_0^{\Delta t} Y_{dd}(0, t) \\
&\qquad \times p_2\mu_2 e^{-\mu_2\tau}d\tau + O(\Delta t^2) \qquad (47)
\end{aligned}
$$

$$\begin{aligned} &Y_{d2}(0, t+\Delta t) \\ &\quad = Y_{d2}(0,t)e^{-(\mu_1+\lambda_{22})\Delta t} \\ &\qquad + \int_0^{c_2\Delta t} X_{22}(h,t)e^{-(\mu_1+\lambda_{22})\Delta t} dh \\ &\qquad + \int_0^{\Delta t} Y_{22}(0,t)\lambda_{12}e^{-\lambda_{12}\tau} d\tau \\ &\qquad + \int_0^{\Delta t} Y_{d1}(0,t)\lambda_{21}e^{-\lambda_{21}\tau} d\tau \\ &\qquad + \int_0^{\Delta t} Y_{dd}(0,t)(1-p_2)\mu_2 e^{-\mu_2\tau} d\tau + O(\Delta t^2) \end{aligned} \tag{48}$$

$$\begin{aligned} &Y_{dd}(0, t+\Delta t) \\ &\quad = Y_{dd}(0,t)e^{-(\mu_1+\mu_2)\Delta t} \\ &\qquad + \int_0^{\Delta t} Y_{d2}(0,t)\lambda_{22}e^{-\lambda_{22}\tau} d\tau + O(\Delta t^2). \end{aligned} \tag{49}$$

The simplified steady-state dynamic equation, following the idea of (11) and (12), is shown as follows:

$$(\lambda_{11}+\lambda_{21})Y_{11}(0) = (c_2-c_1)X_{11}(0)+p_1\mu_1 Y_{d1}(0) \tag{50}$$

$$\begin{aligned} &(\lambda_{11}+\lambda_{22})Y_{12}(0) \\ &\quad = (c_2-c_1)X_{12}(0)+\lambda_{21}Y_{11}(0)+p_1\mu_1 Y_{d2}(0) \end{aligned} \tag{51}$$

$$\lambda_{22}Y_{12}(0)+p_1\mu_1 Y_{dd}(0) = c_1 X_{1d}(0) \tag{52}$$

$$\begin{aligned} &(\lambda_{12}+\lambda_{21})Y_{21}(0) \\ &\quad = (c_2-c_1)X_{21}(0)+\lambda_{11}Y_{11}(0)+(1-p_1)\mu_1 Y_{d1}(0) \end{aligned} \tag{53}$$

$$\begin{aligned} &(\lambda_{12}+\lambda_{22})Y_{22}(0) \\ &\quad = (c_2-c_1)X_{22}(0)+\lambda_{11}Y_{12}(0)+\lambda_{21}Y_{21}(0) \\ &\qquad + (1-p_1)\mu_1 Y_{d2}(0) \end{aligned} \tag{54}$$

$$\lambda_{22}Y_{22}(0)+(1-p_1)\mu_1 Y_{dd}(0) = c_1 X_{2d}(0) \tag{55}$$

$$\begin{aligned} &(\mu_1+\lambda_{21})Y_{d1}(0) \\ &\quad = -c_1 X_{d1}(0)+\lambda_{12}Y_{21}(0)+p_2\mu_2 Y_{dd}(0) \end{aligned} \tag{56}$$

$$\begin{aligned} &(\mu_1+\lambda_{22})Y_{d2}(0) \\ &\quad = -c_1 X_{d2}(0)+\lambda_{12}Y_{22}(0)+\lambda_{21}Y_{d1}(0)+(1-p_2)\mu_2 Y_{dd}(0) \end{aligned} \tag{57}$$

$$(\mu_1+\mu_2)Y_{dd}(0) = \lambda_{22}Y_{d2}(0). \tag{58}$$

The following equations determine the boundary conditions when buffer level is full:

$$\begin{aligned} &Y_{12}(N, t+\Delta t) \\ &\quad = Y_{12}(N,t)e^{-(\lambda_{11}+\lambda_{22})\Delta t} \\ &\qquad + \int_0^{(c_1-c_2)\Delta t} X_{12}(N-h,t)e^{-(\lambda_{11}+\lambda_{22})\Delta t} dh \\ &\qquad + \int_0^{\Delta t} Y_{2d}(N,t)p_1\mu_1 e^{-\mu_1\tau} d\tau + \int_0^{\Delta t} Y_{11}(N,t) \\ &\qquad \times \lambda_{21}e^{-\lambda_{21}\tau} d\tau + O(\Delta t^2) \end{aligned} \tag{59}$$

$$\begin{aligned} &Y_{1d}(N, t+\Delta t) \\ &\quad = Y_{1d}(N,t)e^{-(\mu_2+\lambda_{11})\Delta t} \\ &\qquad + \int_0^{c_2\Delta t} X_{1d}(N,t)e^{-(\mu_2+\lambda_{11})\Delta t} dh \\ &\qquad + \int_0^{\Delta t} Y_{12}(N,t)\lambda_{22}e^{-\lambda_{22}\tau} d\tau + \int_0^{\Delta t} Y_{dd}(N,t) \\ &\qquad \times p_1\mu_1 e^{-\mu_1\tau} d\tau + O(\Delta t^2) \end{aligned} \tag{60}$$

$$\begin{aligned} &Y_{21}(N, t+\Delta t) \\ &\quad = Y_{21}(N,t)e^{-(\lambda_{12}+\lambda_{21})\Delta t} \\ &\qquad + \int_0^{(c_1-c_2)\Delta t} X_{21}(N-h,t)e^{-(\lambda_{12}+\lambda_{21})\Delta t} dh \\ &\qquad + \int_0^{\Delta t} Y_{11}(N,t)\lambda_{11}e^{-\lambda_{11}\tau} d\tau + \int_0^{\Delta t} Y_{d2}(N,t)p_2 \\ &\qquad \times \mu_2 e^{-\mu_2\tau} d\tau + O(\Delta t^2) \end{aligned} \tag{61}$$

$$\begin{aligned} &Y_{22}(N, t+\Delta t) \\ &\quad = Y_{22}(N,t)e^{-(\lambda_{12}+\lambda_{22})\Delta t} \\ &\qquad + \int_0^{(c_2-c_1)\Delta t} X_{22}(N-h,t)e^{-(\lambda_{12}+\lambda_{22})\Delta t} dh \\ &\qquad + \int_0^{\Delta t} Y_{12}(N,t)\lambda_{11}e^{-\lambda_{11}\tau} d\tau + \int_0^{\Delta t} Y_{2d}(N,t)(1-p_2) \\ &\qquad \times \mu_2 e^{-\mu_2\tau} d\tau + \int_0^{\Delta t} Y_{21}(N,t)\lambda_{21}e^{-\lambda_{21}\tau} d\tau + O(\Delta t^2) \end{aligned} \tag{62}$$

$$\begin{aligned} &Y_{2d}(N, t+\Delta t) \\ &\quad = Y_{2d}(N,t)e^{-(\mu_2+\lambda_{22})\Delta t} \\ &\qquad + \int_0^{c_2\Delta t} X_{22}(N-h,t)e^{-(\mu_1+\lambda_{22})\Delta t} dh + \int_0^{\Delta t} Y_{1d}(N,t) \\ &\qquad \times \lambda_{11}e^{-\lambda_{11}\tau} d\tau + \int_0^{\Delta t} Y_{22}(N,t)\lambda_{22}e^{-\lambda_{22}\tau} d\tau \\ &\qquad + \int_0^{\Delta t} Y_{dd}(N,t)(1-p_1)\mu_1 e^{-\mu_1\tau} d\tau + O(\Delta t^2) \end{aligned} \tag{63}$$

$$Y_{d1}(N,t) = 0 \tag{64}$$

$$Y_{d2}(N,t) = 0 \tag{65}$$

$$\begin{aligned} &Y_{dd}(N, t+\Delta t) \\ &\quad = Y_{dd}(N,t)e^{-(\mu_1+\mu_2)\Delta t} \\ &\qquad + \int_0^{\Delta t} Y_{2d}(N,t)\lambda_{22}e^{-\lambda_{22}\tau} d\tau + O(\Delta t^2). \end{aligned} \tag{66}$$

The simplified steady-state dynamic equation, following the idea of (11) and (12), is shown as follows:

$$\begin{aligned} &(\lambda_{11}+\lambda_{21})Y_{11}(N) \\ &\quad = (c_1-c_2)X_{11}(N)+p_2\mu_2 Y_{1d}(N) \end{aligned} \tag{67}$$

$$\begin{aligned} &(\lambda_{11}+\lambda_{22})Y_{12}(N) \\ &\quad = (c_1-c_2)X_{12}(N)+\lambda_{21}Y_{11}(N)+(1-p_2)\mu_2 Y_{1d}(N) \end{aligned} \tag{68}$$

$$\begin{aligned} &(\lambda_{11}+\mu_2)Y_{1d}(N) \\ &\quad = c_1 X_{1d}(N)+\lambda_{22}Y_{12}(N)+p_1\mu_1 Y_{dd}(N) \end{aligned} \tag{69}$$

$$\begin{aligned} &(\lambda_{12}+\lambda_{21})Y_{21}(N) \\ &\quad = (c_1-c_2)X_{21}(N)+\lambda_{22}Y_{12}(N)+p_1\mu_1 Y_{dd}(N) \end{aligned} \tag{70}$$

$$\begin{aligned} &(\lambda_{12}+\lambda_{22})Y_{22}(N) \\ &\quad = (c_1-c_2)X_{22}(N)+\lambda_{11}Y_{12}(N)+\lambda_{21}Y_{21}(N) \\ &\qquad + (1-p_2)\mu_2 Y_{2d}(N) \end{aligned} \tag{71}$$

$$\begin{aligned} &(\lambda_{12}+\lambda_{22})Y_{2d}(N) \\ &\quad = c_1 X_{2d}(N)+\lambda_{22}Y_{22}(N)+(1-p_1)\mu_1 Y_{dd}(N) \end{aligned} \tag{72}$$

$$\lambda_{12}Y_{21}(N)+p_2\mu_2 Y_{dd}(N) = c_2 X_{d1}(N) \tag{73}$$

$$\lambda_{12}Y_{22}(N)+(1-p_2)\mu_2 Y_{dd}(N) = c_2 X_{d2}(N) \tag{74}$$

$$(\mu_1+\mu_2)Y_{dd}(N) = \lambda_{12}Y_{2d}(N). \tag{75}$$

References

[1] F. Ju, J. Li, G. Xiao, J. Arinez, and W. Deng, "Modeling, analysis, and improvement of integrated productivity and quality system in battery manufacturing," *IIE Trans.*, vol. 47, no. 12, pp. 1313–1328, Jun. 2015.

[2] Y. Kang and F. Ju, "Integrated analysis of productivity and machine condition degradation: A geometric-machine case," in *Proc. IEEE Int. Conf. Autom. Sci. Eng. (CASE)*, Aug. 2016, pp. 1128–1133.

[3] Y. Lu and F. Ju, "Smart manufacturing systems based on cyber-physical manufacturing services (CPMS)," *IFAC-PapersOnLine*, vol. 50, no. 1, pp. 15883–15889, Jul. 2017.

[4] N. Z. Gebraeel, M. A. Lawley, R. Li, and J. K. Ryan, "Residual-life distributions from component degradation signals: A Bayesian approach," *IIE Trans.*, vol. 37, no. 6, pp. 543–557, Feb. 2005.

[5] J. Li and S. M. Meerkov, *Production Systems Engineering*. New York, NY, USA: Springer, 2008.

[6] M. D. Mascolo, R. David, and Y. Dallery, "Modeling and analysis of assembly systems with unreliable machines and finite buffers," *IIE Trans.*, vol. 23, no. 4, pp. 315–330, May 1991.

[7] J. A. Buzacott and J. G. Shanthikumar, *Stochastic Modeling of Manufacturing Systems*, vol. 4. Englewood Cliffs, NJ, USA: Prentice-Hall, 1993.

[8] H. Tempelmeier and M. Bürger, "Performance evaluation of unbalanced flow lines with general distributed processing times, failures and imperfect production," *IIE Trans.*, vol. 33, no. 4, pp. 293–302, Apr. 2001.

[9] D. Jacobs and S. M. Meerkov, "System-theoretic analysis of due-time performance in production systems," *Math. Problems Eng.*, vol. 1, no. 3, pp. 225–243, 1995.

[10] J. Li, D. E. Blumenfeld, N. Huang, and J. M. Alden, "Throughput analysis of production systems: Recent advances and future topics," *Int. J. Prod. Res.*, vol. 47, no. 14, pp. 3823–3851, May 2009.

[11] S.-Y. Chiang, C.-T. Kuo, J.-T. Lim, and S. Meerkov, "Improvability of assembly systems I: Problem formulation and performance evaluation," *Math. Problems Eng.*, vol. 6, no. 4, pp. 321–357, 2000.

[12] R. R. Inman, "Empirical evaluation of exponential and independence assumptions in queueing models of manufacturing systems," *Prod. Oper. Manage.*, vol. 8, no. 4, pp. 409–432, Dec. 1999.

[13] J. Li and S. M. Meerkov, "On the coefficients of variation of uptime and downtime in manufacturing equipment," *Math. Problems Eng.*, vol. 2005, no. 1, pp. 1–6, 2005.

[14] J. Zhou, D. Djurdjanovic, J. Ivy, and J. Ni, "Integrated reconfiguration and age-based preventive maintenance decision making," *IIE Trans.*, vol. 39, no. 12, pp. 1085–1102, Nov. 2007.

[15] M. Colledani and T. Tolio, "Integrated quality, production logistics and maintenance analysis of multi-stage asynchronous manufacturing systems with degrading machines," *CIRP Ann.*, vol. 61, no. 1, pp. 455–458, 2012.

[16] O. A. Arik and M. D. Toksari, "Multi-objective fuzzy parallel machine scheduling problems under fuzzy job deterioration and learning effects," *Int. J. Prod. Res.*, vol. 56, no. 7, pp. 2488–2505, Oct. 2018.

[17] X. Zhang, W.-H. Wu, W.-C. Lin, and C.-C. Wu, "Machine scheduling problems under deteriorating effects and deteriorating rate-modifying activities," *J. Oper. Res. Soc.*, vol. 69, no. 3, pp. 439–448, Jan. 2018.

[18] P. Renna, "Deteriorating job scheduling problem in a job-shop manufacturing system by multi-agent system," *Int. J. Comput. Integr. Manuf.*, vol. 28, no. 9, pp. 936–945, Jul. 2015.

[19] G. Chen, C. Wang, L. Zhang, J. Arinez, and G. Xiao, "Transient performance analysis of serial production lines with geometric machines," *IEEE Trans. Autom. Control*, vol. 61, no. 4, pp. 877–891, Apr. 2016.

[20] Z. Jia, L. Zhang, J. Arinez, and G. Xiao, "Finite production run-based serial lines with Bernoulli machines: Performance analysis, bottleneck, and case study," *IEEE Trans. Autom. Sci. Eng.*, vol. 13, no. 1, pp. 134–148, Jan. 2016.

[21] L. Bian and N. Gebraeel, "Stochastic modeling and real-time prognostics for multi-component systems with degradation rate interactions," *IIE Trans.*, vol. 46, no. 5, pp. 470–482, Feb. 2014.

[22] J. Zou, Q. Chang, J. Arinez, G. Xiao, and Y. Lei, "Dynamic production system diagnosis and prognosis using model-based data-driven method," *Expert Syst. With Appl.*, vol. 80, pp. 200–209, Sep. 2017.

[23] J. Zou, Q. Chang, Y. Lei, and J. Arinez, "Production system performance identification using sensor data," *IEEE Trans. Syst., Man, Cybern. Syst.*, vol. 48, no. 2, pp. 255–264, Feb. 2018.

[24] C. J. Lu and W. O. Meeker, "Using degradation measures to estimate a time-to-failure distribution," *Technometrics*, vol. 35, no. 2, pp. 161–174, Mar. 1993.

[25] M. J. Zuo, R. Jiang, and R. C. M. Yam, "Approaches for reliability modeling of continuous-state devices," *IEEE Trans. Rel.*, vol. 48, no. 1, pp. 9–18, Mar. 1999.

[26] M. Zhang, O. Gaudoin, and M. Xie, "Degradation-based maintenance decision using stochastic filtering for systems under imperfect maintenance," *Eur. J. Oper. Res.*, vol. 245, no. 2, pp. 531–541, Sep. 2015.

[27] K. Liu, N. Z. Gebraeel, and J. Shi, "A data-level fusion model for developing composite health indices for degradation modeling and prognostic analysis," *IEEE Trans. Autom. Sci. Eng.*, vol. 10, no. 3, pp. 652–664, Jul. 2013.

[28] H. Yan, K. Liu, X. Zhang, and J. Shi, "Multiple sensor data fusion for degradation modeling and prognostics under multiple operational conditions," *IEEE Trans. Rel.*, vol. 65, no. 3, pp. 1416–1426, Sep. 2016.

[29] L. Hao, K. Liu, N. Gebraeel, and J. Shi, "Controlling the residual life distribution of parallel unit systems through workload adjustment," *IEEE Trans. Autom. Sci. Eng.*, vol. 14, no. 2, pp. 1042–1052, Apr. 2017.

[30] K. A. Doksum and A. Hbyland, "Models for variable-stress accelerated life testing experiments based on wener processes and the inverse Gaussian distribution," *Technometrics*, vol. 34, no. 1, pp. 74–82, Mar. 1992.

[31] H. Okamura, T. Dohi, and K. S. Trivedi, "A refined EM algorithm for PH distributions," *Perform. Eval.*, vol. 68, no. 10, pp. 938–954, Oct. 2011.

[32] M. P. Blake and W. S. Mitchell, *Vibration and Acoustic Measurement Handbook*. Washington, DC, USA: Spartan Books, 1972.

Yunyi Kang (S'14) received the B.S. degree from the Department of Industrial Systems and Engineering, The Hong Kong Polytechnic University, Hong Kong, and the M.S. degree from the Department of Industrial Systems and Engineering, Rutgers University, New Brunswick, NJ, USA, in 2013 and 2015, respectively. He is currently pursuing the Ph.D. degree at the School of Computing, Informatics, and Decision Systems Engineering, Arizona State University, Tempe, AZ, USA.

His research interests are in modeling, analysis, and real-time control of production systems.

Mr. Kang was a recipient of the Best Student Paper Finalist in IEEE CASE.

Hao Yan received the B.S. degree in physics from Peking University, Beijing, China, in 2011, and the M.S. degree in statistics, the M.S. degree in computational science and engineering, and the Ph.D. degree in industrial engineering from the Georgia Institute of Technology, Atlanta, GA, USA, in 2015, 2016, and 2017, respectively.

He is currently an Assistant Professor with the School of Computing, Informatics, and Decision Systems Engineering, Arizona State University, Tempe, AZ, USA. His research interests focus on developing scalable statistical learning algorithms for large-scale high-dimensional data with complex heterogeneous structures to extract useful information for the purpose of system performance assessment, anomaly detection, intelligent sampling, and decision-making.

Dr. Yan is a member of INFORMS and IIE.

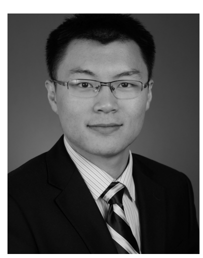

Feng Ju (M'15) received the B.S. degree from Shanghai Jiao Tong University, Shanghai, China, in 2010, and the M.S. degree in electrical and computer engineering and the Ph.D. degree in industrial and systems engineering from the University of Wisconsin, Madison, WI, USA, in 2011 and 2015, respectively.

He is currently an Assistant Professor with the School of Computing, Informatics, and Decision Systems Engineering, Arizona State University, Tempe, AZ, USA. His current research interests include modeling, analysis, continuous improvement, and optimization of manufacturing systems.

Dr. Ju is a member of the Institute for Operations Research and the Management Sciences and the Institute of Industrial Engineers. He was a recipient of multiple awards, including the Best Paper Award in IFAC MIM and the Best Student Paper Finalist in IEEE CASE and IFAC INCOM.